Journal of Advances in Modeling Earth Systems

Supporting Information for

Enhanced snow absorption and albedo reduction by dust-snow internal mixing: modeling and parameterization

Cenlin He[1,2], Kuo-Nan Liou[3], Yoshi Takano[3], Fei Chen[2], Michael Barlage[2]

[1]Advanced Study Program, National Center for Atmospheric Research, Boulder, CO, USA

[2]Research Applications Laboratory, National Center for Atmospheric Research, Boulder, CO, USA

[3]Department of Atmospheric and Oceanic Sciences, and Joint Institute for Regional Earth System Science and Engineering, University of California, Los Angeles, CA, USA

Corresponding author: Cenlin He (cenlinhe@ucar.edu)

Contents of this file

Table S1. Parameterization coefficients (Equations 2–3) for snow albedo reductions ($\Delta\alpha$) caused by dust-snow internal and external mixing for the Community Land Model (CLM) bands.

Snow grain shape	Wavelength bands (μm)*	Clear sky			Overcast cloud		
		b_1	b_2	b_3	b_1	b_2	b_3
Dust-snow internal mixing							
Sphere	0.3–0.7	1.9645E-02	3.6062E-01	1.3040E-01	2.0192E-02	3.5836E-01	1.3089E-01
	0.7–1.0	9.2463E-04	6.5854E-01	6.9980E-02	9.5387E-04	6.5614E-01	7.0398E-02
	1.0–1.2	4.3674E-05	9.3644E-01	3.1950E-02	4.4552E-05	9.3489E-01	3.2358E-02
	1.2–1.5	5.6980E-06	1.0768E+00	-5.9752E-03	6.0247E-06	1.0814E+00	-5.2865E-03
Spheroid	0.3–0.7	1.9082E-02	3.6058E-01	1.3625E-01	1.9629E-02	3.5825E-01	1.3677E-01
	0.7–1.0	8.9180E-04	6.4222E-01	8.5898E-02	9.2239E-04	6.3999E-01	8.6103E-02
	1.0–1.2	1.6955E-05	1.0016E+00	5.6448E-02	1.7613E-05	9.9690E-01	5.7137E-02
	1.2–1.5	2.9939E-04	2.5726E-01	1.8436E-01	3.3211E-04	2.5221E-01	1.8938E-01
Hexagonal Plate	0.3–0.7	1.3728E-02	3.8436E-01	1.3842E-01	1.4133E-02	3.8197E-01	1.3900E-01
	0.7–1.0	3.7748E-04	7.4696E-01	7.2666E-02	3.9559E-04	7.4256E-01	7.3349E-02
	1.0–1.2	1.9000E-07	1.6337E+00	1.5071E-02	2.1020E-07	1.6223E+00	1.6311E-02
	1.2–1.5	8.8023E-15	1.8804E+00	-2.3128E+00	8.6412E-15	1.7336E+00	-2.6805E+00
Koch Snowflake	0.3–0.7	1.2785E-02	3.8758E-01	1.4141E-01	1.3137E-02	3.8548E-01	1.4192E-01
	0.7–1.0	1.1951E-03	5.8159E-01	9.5502E-02	1.2017E-03	5.8281E-01	9.5628E-02
	1.0–1.2	3.9159E-03	2.6510E-01	1.2790E-01	3.7770E-03	2.7186E-01	1.2909E-01
	1.2–1.5	8.0743E-03	9.0914E-02	8.2155E-02	8.3234E-03	9.3168E-02	1.2329E-01
Dust-snow external mixing							
Sphere	0.3–0.7	2.0143E-02	3.4101E-01	1.3412E-01	2.0684E-02	3.3891E-01	1.3475E-01
	0.7–1.0	9.9920E-04	6.2275E-01	5.1957E-02	1.0293E-03	6.2082E-01	5.3049E-02
	1.0–1.2	-	-	-	-	-	-
	1.2–1.5	-	-	-	-	-	-
Spheroid	0.3–0.7	1.5426E-02	3.6322E-01	1.3106E-01	1.5870E-02	3.6094E-01	1.3174E-01
	0.7–1.0	5.5732E-04	6.7658E-01	4.6484E-02	5.7654E-04	6.7421E-01	4.7675E-02
	1.0–1.2	-	-	-	-	-	-
	1.2–1.5	-	-	-	-	-	-
Hexagonal Plate	0.3–0.7	1.1981E-02	3.8004E-01	1.3452E-01	1.2324E-02	3.7782E-01	1.3518E-01
	0.7–1.0	4.6142E-04	6.8322E-01	5.4576E-02	4.7695E-04	6.8097E-01	5.5640E-02
	1.0–1.2	-	-	-	-	-	-
	1.2–1.5	-	-	-	-	-	-
Koch Snowflake	0.3–0.7	1.0425E-02	3.8807E-01	1.3562E-01	1.0720E-02	3.8592E-01	1.3627E-01
	0.7–1.0	4.2734E-04	6.8311E-01	5.7785E-02	4.4159E-04	6.8087E-01	5.8823E-02
	1.0–1.2	-	-	-	-	-	-
	1.2–1.5	-	-	-	-	-	-

*We do not parameterize for dust-snow external mixing at wavelengths of 1.0–1.5 μm, due to negligible snow albedo reduction in these cases. The last CLM band (1.5–5.0 μm) is also not shown for both dust-snow internal and external mixing, due to negligible dust-induced albedo reduction.

Table S2. Parameterization coefficients (Equations 2–3) for snow albedo reductions ($\Delta\alpha$) caused by dust-snow internal and external mixing for the Fu-Liou bands.

Snow grain shape	Wavelength bands (μm)*	Clear sky			Overcast cloud		
		b_1	b_2	b_3	b_1	b_2	b_3
Dust-snow internal mixing							
Sphere	0.2–0.7	1.9645E-02	3.6062E-01	1.3040E-01	2.0192E-02	3.5836E-01	1.3089E-01
	0.7–1.3	5.8256E-04	6.8349E-01	6.4133E-02	6.1561E-04	6.7953E-01	6.4906E-02
	1.3–1.9	1.1805E-06	1.0415E+00	-1.2324E-02	9.4497E-07	1.0440E+00	-1.2063E-02
Spheroid	0.2–0.7	1.9082E-02	3.6058E-01	1.3625E-01	1.9629E-02	3.5825E-01	1.3677E-01
	0.7–1.3	5.6627E-04	6.5878E-01	8.3896E-02	6.0028E-04	6.5531E-01	8.4291E-02
	1.3–1.9	4.8645E-05	2.7448E-01	1.6171E-01	4.0926E-05	2.6860E-01	1.6442E-01
Hexagonal Plate	0.2–0.7	1.3728E-02	3.8436E-01	1.3842E-01	1.4133E-02	3.8198E-01	1.3900E-01
	0.7–1.3	2.1860E-04	7.7648E-01	6.7570E-02	2.3561E-04	7.7057E-01	6.8561E-02
	1.3–1.9	9.8656E-26	1.7864E-01	2.1526E-01	9.8656E-26	1.7864E-01	2.1526E-01
Koch Snowflake	0.2–0.7	1.2785E-02	3.8758E-01	1.4141E-01	1.3137E-02	3.8548E-01	1.4192E-01
	0.7–1.3	1.3699E-03	5.2507E-01	9.8605E-02	1.3518E-03	5.3064E-01	9.8564E-02
	1.3–1.9	3.9898E-03	4.3176E-02	-3.4879E+00	3.6810E-03	2.6065E-02	-5.1631E+00
Dust-snow external mixing							
Sphere	0.2–0.7	2.0143E-02	3.4101E-01	1.3412E-01	2.0684E-02	3.3891E-01	1.3475E-01
	0.7–1.3	6.7078E-04	6.3056E-01	3.3671E-02	7.0479E-04	6.2827E-01	3.6275E-02
	1.3–1.9	-	-	-	-	-	-
Spheroid	0.2–0.7	1.5426E-02	3.6322E-01	1.3106E-01	1.5870E-02	3.6094E-01	1.3174E-01
	0.7–1.3	3.5280E-04	6.9037E-01	2.5903E-02	3.7420E-04	6.8708E-01	2.8878E-02
	1.3–1.9	-	-	-	-	-	-
Hexagonal Plate	0.2–0.7	1.1981E-02	3.8004E-01	1.3452E-01	1.2324E-02	3.7782E-01	1.3518E-01
	0.7–1.3	2.9130E-04	6.9716E-01	3.4131E-02	3.0882E-04	6.9400E-01	3.6928E-02
	1.3–1.9	-	-	-	-	-	-
Koch Snowflake	0.2–0.7	1.0425E-02	3.8807E-01	1.3562E-01	1.0720E-02	3.8592E-01	1.3627E-01
	0.7–1.3	2.6854E-04	6.9734E-01	3.5724E-02	2.8473E-04	6.9420E-01	3.8629E-02
	1.3–1.9	-	-	-	-	-	-

*We do not parameterize for dust-snow external mixing at the wavelength band of 1.3–1.9 μm, due to negligible snow albedo reduction in these cases. The last three Fu-Liou bands (i.e., 1.9–2.5, 2.5–3.5, 3.5–4.0 μm) are also not shown for both dust-snow internal and external mixing, due to negligible dust-induced albedo reduction.

Table S3. Parameterization coefficients (Equations 2–3) for snow albedo reductions ($\Delta\alpha$) caused by dust-snow internal and external mixing for the Rapid Radiative Transfer Model (RRTM) bands.

Snow grain shape	Wavelength bands (μm)*	Clear sky			Overcast cloud		
		b_1	b_2	b_3	b_1	b_2	b_3
		Dust-snow internal mixing					
Sphere	0.2000–0.2632	6.7602E-02	2.7725E-01	1.3547E-01	6.7602E-02	2.7725E-01	1.3547E-01
	0.2632–0.3448	5.3865E-02	2.9097E-01	1.3890E-01	5.3861E-02	2.9098E-01	1.3890E-01
	0.3448–0.4415	4.0041E-02	3.0866E-01	1.4148E-01	4.0186E-02	3.0844E-01	1.4146E-01
	0.4415–0.6250	1.7955E-02	3.6765E-01	1.3183E-01	1.8084E-02	3.6702E-01	1.3200E-01
	0.6250–0.7782	3.7562E-03	5.2311E-01	9.4331E-02	3.8043E-03	5.2177E-01	9.4605E-02
	0.7782–1.2422	3.0868E-04	7.5149E-01	5.5229E-02	3.2762E-04	7.4674E-01	5.6013E-02
	1.2422–1.2987	6.1085E-06	1.0813E+00	-5.7285E-03	6.1068E-06	1.0814E+00	-5.7142E-03
	1.2987–1.6260	2.2578E-06	1.0469E+00	-1.1502E-02	2.1614E-06	1.0520E+00	-1.0836E-02
Spheroid	0.2000–0.2632	6.9332E-02	2.7350E-01	1.4225E-01	6.9332E-02	2.7350E-01	1.4225E-01
	0.2632–0.3448	5.3560E-02	2.8928E-01	1.4583E-01	5.3556E-02	2.8928E-01	1.4583E-01
	0.3448–0.4415	3.9707E-02	3.0665E-01	1.4866E-01	3.9854E-02	3.0642E-01	1.4864E-01
	0.4415–0.6250	1.7290E-02	3.6889E-01	1.3677E-01	1.7416E-02	3.6826E-01	1.3694E-01
	0.6250–0.7782	3.5793E-03	5.2099E-01	1.0315E-01	3.6236E-03	5.1978E-01	1.0335E-01
	0.7782–1.2422	2.6978E-04	7.3471E-01	7.5413E-02	2.8907E-04	7.2972E-01	7.5856E-02
	1.2422–1.2987	4.4795E-04	2.0373E-01	2.3080E-01	4.4822E-04	2.0362E-01	2.3097E-01
	1.2987–1.6260	1.0217E-04	2.6319E-01	1.6884E-01	1.0673E-04	2.5287E-01	1.7520E-01
Hexagonal Plate	0.2000–0.2632	5.3513E-02	2.9592E-01	1.4737E-01	5.3513E-02	2.9592E-01	1.4737E-01
	0.2632–0.3448	3.9482E-02	3.1297E-01	1.5131E-01	3.9479E-02	3.1298E-01	1.5131E-01
	0.3448–0.4415	2.9014E-02	3.2980E-01	1.5275E-01	2.9125E-02	3.2958E-01	1.5275E-01
	0.4415–0.6250	1.2380E-02	3.9279E-01	1.3810E-01	1.2472E-02	3.9214E-01	1.3827E-01
	0.6250–0.7782	2.2911E-03	5.6070E-01	1.0074E-01	2.3248E-03	5.5913E-01	1.0103E-01
	0.7782–1.2422	7.6531E-05	8.9949E-01	5.5289E-02	8.4401E-05	8.9028E-01	5.6515E-02
	1.2422–1.2987	9.8656E-26	1.7864E-01	2.1526E-01	9.8656E-26	1.7864E-01	2.1526E-01
	1.2987–1.6260	1.6461E-26	8.7594E-02	1.1039E-01	1.6461E-26	8.7594E-02	1.1039E-01
Koch Snowflake	0.2000–0.2632	4.6445E-02	3.0837E-01	1.4985E-01	4.6445E-02	3.0837E-01	1.4985E-01
	0.2632–0.3448	3.5180E-02	3.2290E-01	1.5340E-01	3.5177E-02	3.2290E-01	1.5340E-01
	0.3448–0.4415	2.6021E-02	3.3878E-01	1.5425E-01	2.6119E-02	3.3856E-01	1.5426E-01
	0.4415–0.6250	1.1474E-02	3.9649E-01	1.4056E-01	1.1554E-02	3.9592E-01	1.4070E-01
	0.6250–0.7782	2.7767E-03	5.2672E-01	1.0986E-01	2.8062E-03	5.2571E-01	1.1008E-01
	0.7782–1.2422	1.2740E-03	5.1255E-01	9.6891E-02	1.2384E-03	5.2018E-01	9.6777E-02
	1.2422–1.2987	8.6623E-03	9.4440E-02	1.3827E-01	8.6597E-03	9.4505E-02	1.3856E-01
	1.2987–1.6260	4.8719E-03	7.3649E-02	-1.1028E+00	4.8165E-03	7.4456E-02	-1.0886E+00

Table S3. (continued)

Snow grain shape	Wavelength bands (μm)*	Clear sky			Overcast cloud		
		b_1	b_2	b_3	b_1	b_2	b_3
		Dust-snow external mixing					
Sphere	0.2000–0.2632	6.5046E-02	2.6606E-01	1.4618E-01	6.5046E-02	2.6606E-01	1.4618E-01
	0.2632–0.3448	5.2751E-02	2.7835E-01	1.4784E-01	5.2747E-02	2.7835E-01	1.4784E-01
	0.3448–0.4415	4.0057E-02	2.9310E-01	1.4918E-01	4.0192E-02	2.9291E-01	1.4917E-01
	0.4415–0.6250	1.8486E-02	3.4768E-01	1.3480E-01	1.8615E-02	3.4708E-01	1.3501E-01
	0.6250–0.7782	3.9956E-03	4.9569E-01	9.0579E-02	4.0462E-03	4.9440E-01	9.0914E-02
	0.7782–1.2422	3.3819E-04	7.0148E-01	5.8286E-03	3.5833E-04	6.9798E-01	9.6332E-03
	1.2422–1.2987	-	-	-	-	-	-
	1.2987–1.6260	-	-	-	-	-	-
Spheroid	0.2000–0.2632	5.1747E-02	2.8703E-01	1.4410E-01	5.1747E-02	2.8703E-01	1.4410E-01
	0.2632–0.3448	4.2023E-02	2.9784E-01	1.4632E-01	4.2020E-02	2.9784E-01	1.4632E-01
	0.3448–0.4415	3.1984E-02	3.1141E-01	1.4756E-01	3.2093E-02	3.1123E-01	1.4756E-01
	0.4415–0.6250	1.4004E-02	3.7142E-01	1.3094E-01	1.4112E-02	3.7074E-01	1.3117E-01
	0.6250–0.7782	2.5916E-03	5.3510E-01	8.6218E-02	2.6276E-03	5.3370E-01	8.6548E-02
	0.7782–1.2422	1.4632E-04	7.8481E-01	-6.8609E-03	1.5833E-04	7.7881E-01	-2.1994E-03
	1.2422–1.2987	-	-	-	-	-	-
	1.2987–1.6260	-	-	-	-	-	-
Hexagonal Plate	0.2000–0.2632	4.0759E-02	3.0634E-01	1.4767E-01	4.0759E-02	3.0634E-01	1.4767E-01
	0.2632–0.3448	3.2541E-02	3.1730E-01	1.4965E-01	3.2538E-02	3.1730E-01	1.4965E-01
	0.3448–0.4415	2.4740E-02	3.2997E-01	1.5047E-01	2.4825E-02	3.2980E-01	1.5047E-01
	0.4415–0.6250	1.0877E-02	3.8777E-01	1.3422E-01	1.0961E-02	3.8711E-01	1.3444E-01
	0.6250–0.7782	2.0595E-03	5.4738E-01	9.1229E-02	2.0875E-03	5.4602E-01	9.1542E-02
	0.7782–1.2422	1.2754E-04	7.8301E-01	6.5713E-03	1.3757E-04	7.7764E-01	1.0598E-02
	1.2422–1.2987	-	-	-	-	-	-
	1.2987–1.6260	-	-	-	-	-	-
Koch Snowflake	0.2000–0.2632	3.5172E-02	3.1800E-01	1.4850E-01	3.5172E-02	3.1800E-01	1.4850E-01
	0.2632–0.3448	2.8014E-02	3.2789E-01	1.5094E-01	2.8012E-02	3.2789E-01	1.5095E-01
	0.3448–0.4415	2.1366E-02	3.3956E-01	1.5139E-01	2.1438E-02	3.3940E-01	1.5139E-01
	0.4415–0.6250	9.4787E-03	3.9536E-01	1.3514E-01	9.5503E-03	3.9472E-01	1.3535E-01
	0.6250–0.7782	1.8497E-03	5.5064E-01	9.3383E-02	1.8743E-03	5.4931E-01	9.3686E-02
	0.7782–1.2422	1.2062E-04	7.7955E-01	9.8823E-03	1.3004E-04	7.7436E-01	1.3888E-02
	1.2422–1.2987	-	-	-	-	-	-
	1.2987–1.6260	-	-	-	-	-	-

*We do not parameterize for dust-snow external mixing at wavelength bands of 1.2422–1.6260 μm, due to negligible snow albedo reduction in these cases. The last six RRTM bands (i.e., 1.6260–1.9417, 1.9417–2.1505, 2.1505–2.5000, 2.5000–3.0769, 3.0769–3.8462, 3.8462–12.1951 μm) are also not shown for both dust-snow internal and external mixing, due to negligible dust-induced albedo reduction.

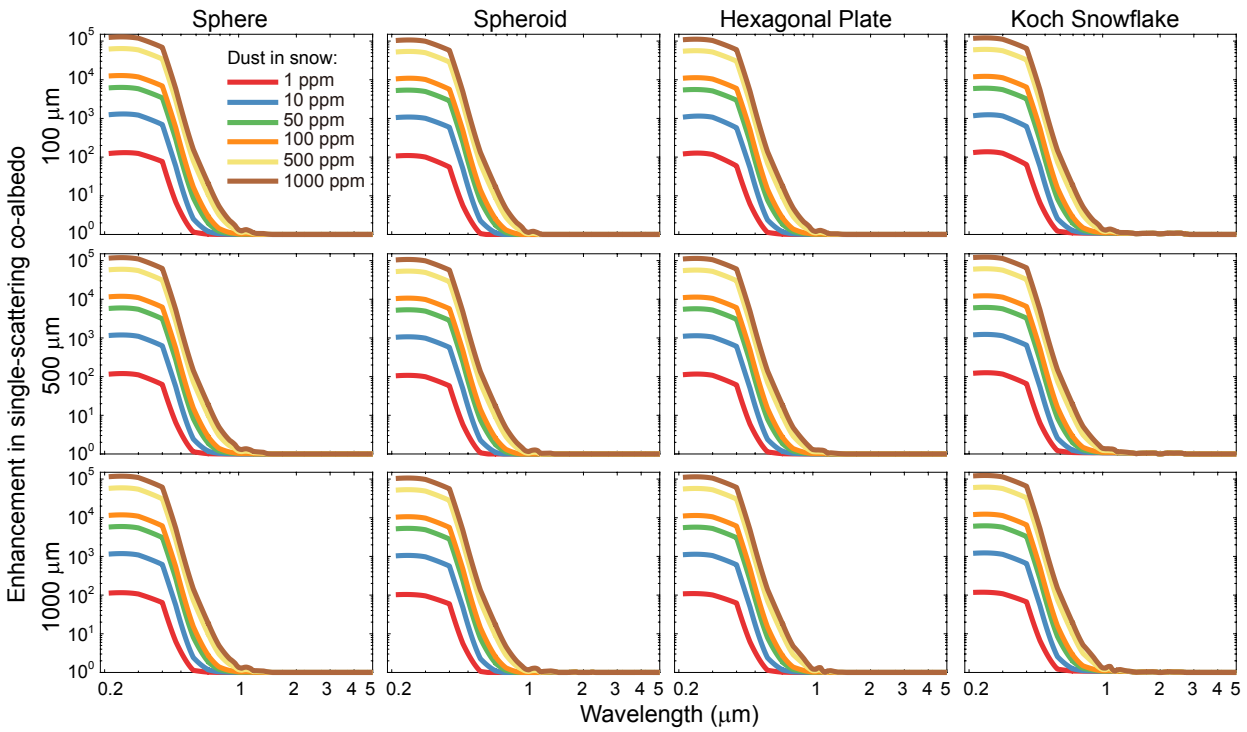

Figure S1. Spectral single-scattering co-albedo enhancement (see text for definition) caused by dust-snow internal mixing from reference calculations for different dust concentrations in snow (indicated by different colors), with snow volume-equivalent sphere radii of 100 μm (top row), 500 μm (middle row), and 1000 μm (bottom row) for sphere (1st column), spheroid (2nd column), hexagonal plate (3rd column), and Koch snowflake (4th column).

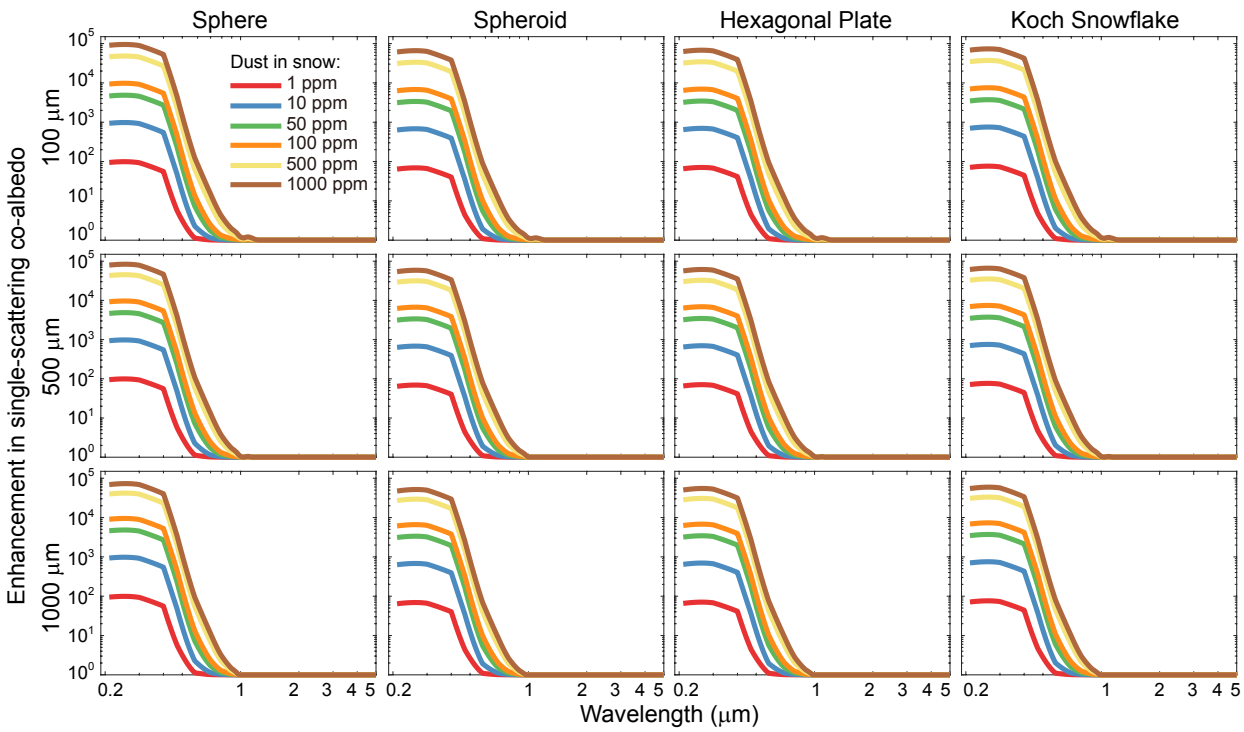

Figure S2. Same as Figure S1, but for dust-snow external mixing.

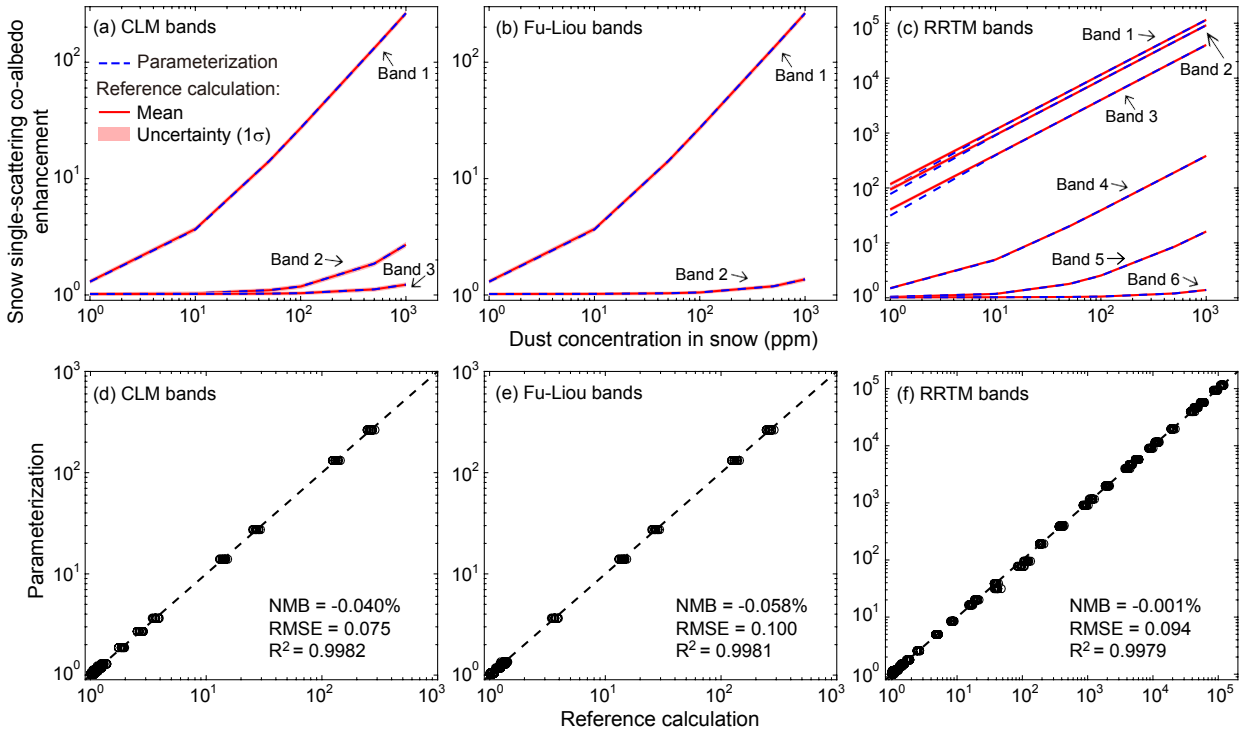

Figure S3. (a–c) Single-scattering co-albedo enhancement ($E_{1\text{-}\omega}$; see text for definition) under the overcast-cloud condition caused by dust-snow internal mixing as a function of dust concentration in snow from reference calculations (red) and parameterizations (Equation 1; blue dashed lines) at different wavelength bands, including (a) the Community Land Model (CLM) bands, (b) the Fu-Liou bands, and (c) the Rapid Radiative Transfer Model (RRTM) bands. Results at wavelength bands of > ~1.2 μm are not shown due to negligible dust effects on $E_{1\text{-}\omega}$. The red lines and shaded areas are, respectively, the mean and one standard deviation (1σ) uncertainty range based on reference calculations using different snow grain shapes (i.e., sphere, spheroid, hexagonal plate, and Koch snowflake) and volume-equivalent sphere radii (i.e., 100, 500, and 1000 μm). Note that the red solid lines and blue dashed lines are almost overlapped in all cases because of very close values, and the uncertainty (shaded area) is rather small due to very small effects of variabilities in snow grain shape and size on $E_{1\text{-}\omega}$ (as opposed to the large effects of dust content variabilities on $E_{1\text{-}\omega}$). (d–f) Comparisons of dust-induced overcast-cloud single-scattering co-albedo enhancement ($E_{1\text{-}\omega}$) from reference calculations and parameterizations at the (d) CLM, (e) Fu-Liou, and (f) RRTM bands based on the results shown in (a–c). Also shown are the normalized mean bias (NMB), the root-mean-square-error (RMSE) normalized by standard deviations of reference calculations, and the coefficient of determination (R^2).

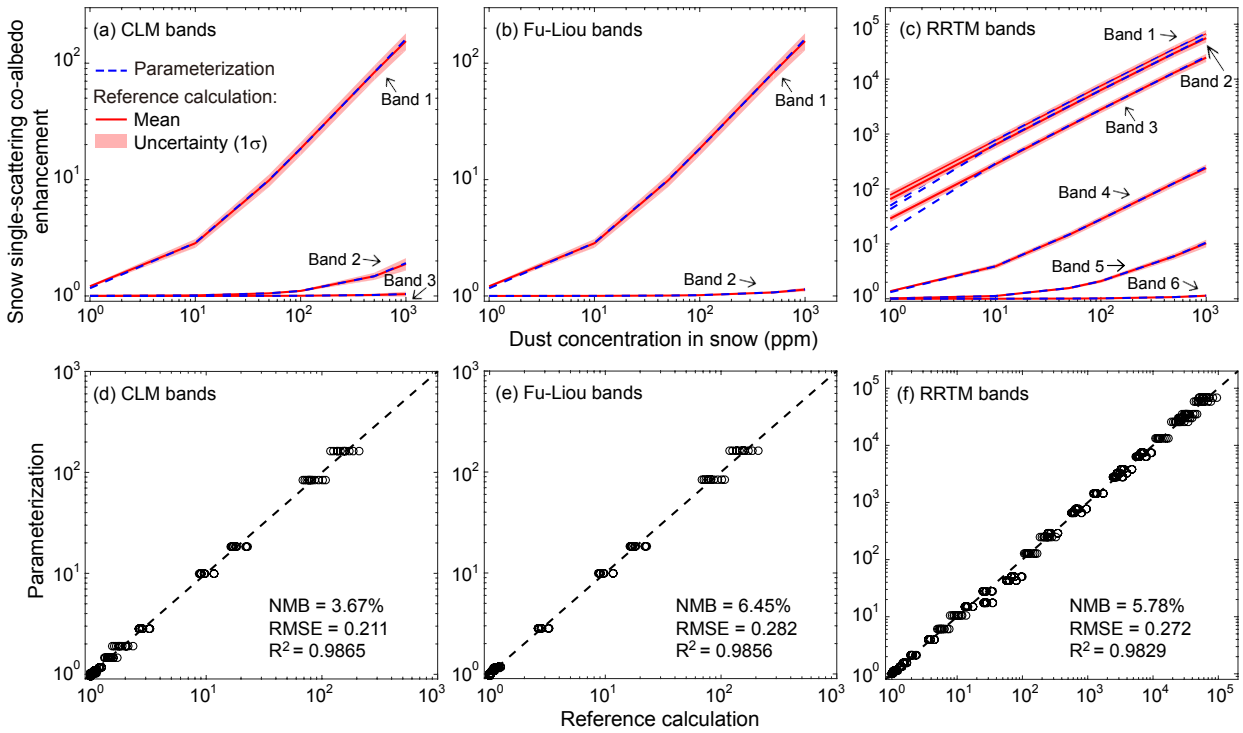

Figure S4. Same as Figure S3, but for dust-snow external mixing under the clear-sky condition.

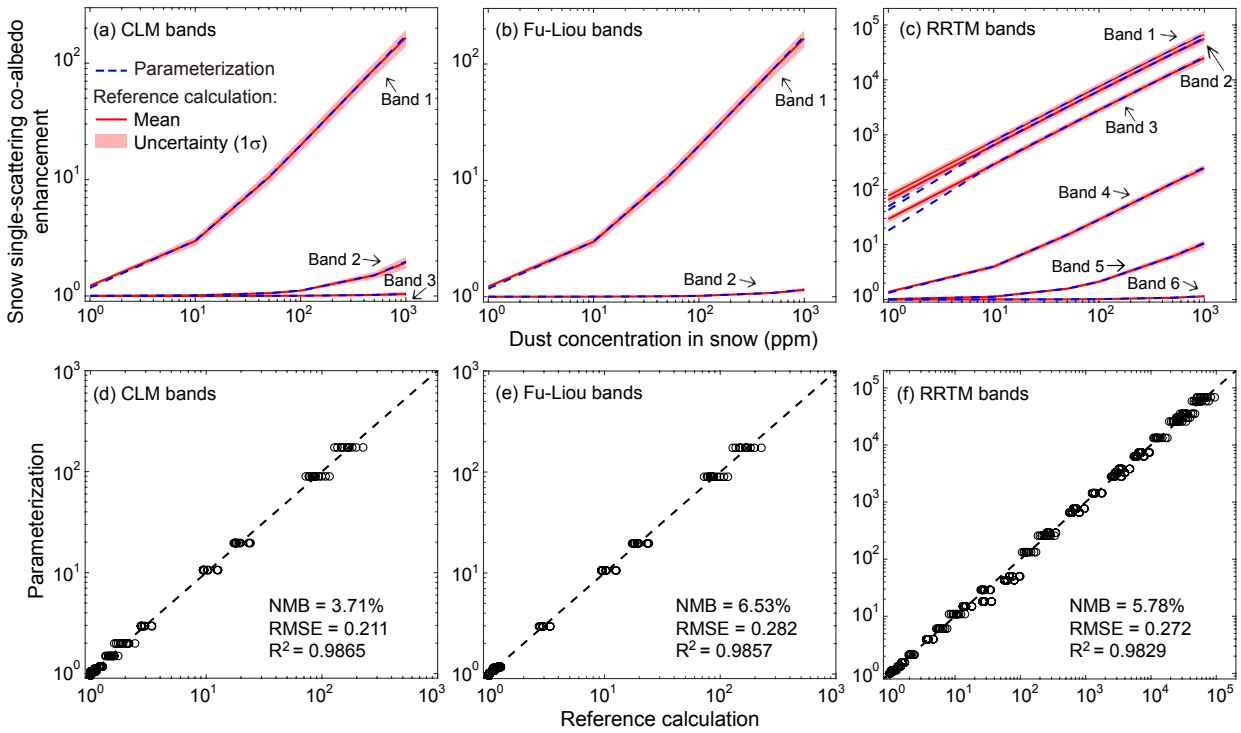

Figure S5. Same as Figure S3, but for dust-snow external mixing under the overcast-cloud condition.

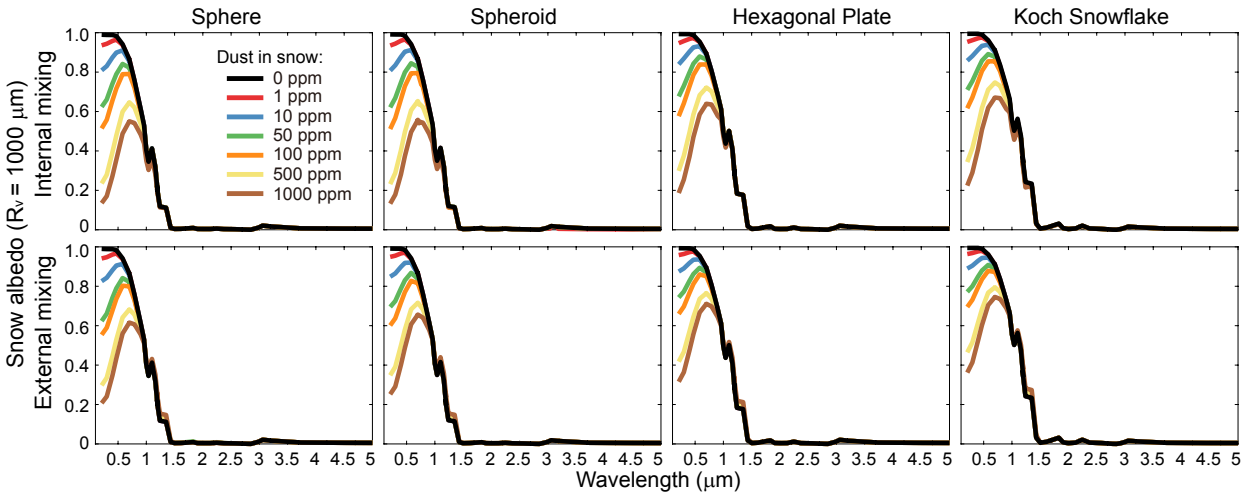

Figure S6. Spectral snow albedo from reference calculations for clean (black lines) and dust-contaminated snow (colored lines) with a volume-equivalent sphere radius (R_v) of 1000 mm and four snow grain shapes, including sphere (1st column), spheroid (2nd column), hexagonal plate (3rd column), and Koch snowflake (4th column), for dust-snow internal (top row) and external (bottom row) mixing.

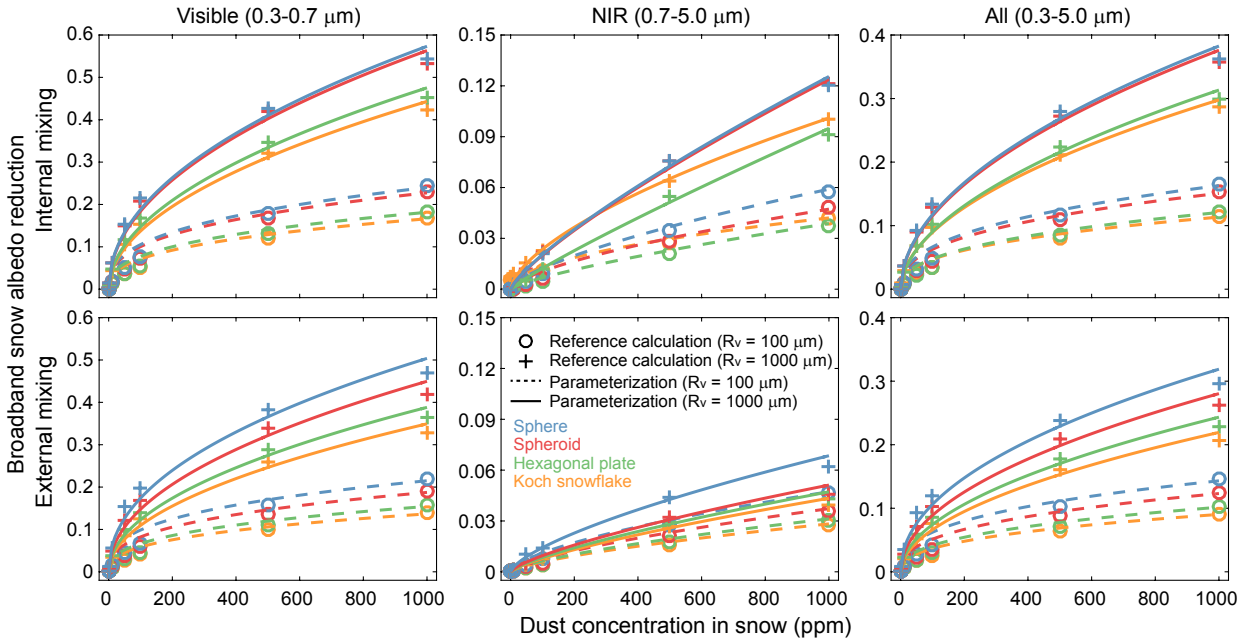

Figure S7. Broadband snow albedo reduction ($\Delta\alpha$) under the overcast-cloud condition as a function of dust concentration in snow from reference calculations (points) and parameterizations (Equations 2–4; lines) for dust-snow internal (top row) and external (bottom row) mixing at the visible (0.3–0.7 μm; 1st column), near-infrared (NIR, 0.7–5.0 μm; 2nd column), and all-wavelength (All, 0.3–5.0 μm; 3rd column) bands. Results shown here are for snow volume-equivalent sphere radii (R_v) of 100 μm (circles or dashed lines) and 1000 μm (crosses or solid lines) and four grain shapes, including sphere (blue), spheroid (red), hexagonal plate (green), and Koch snowflake (orange).

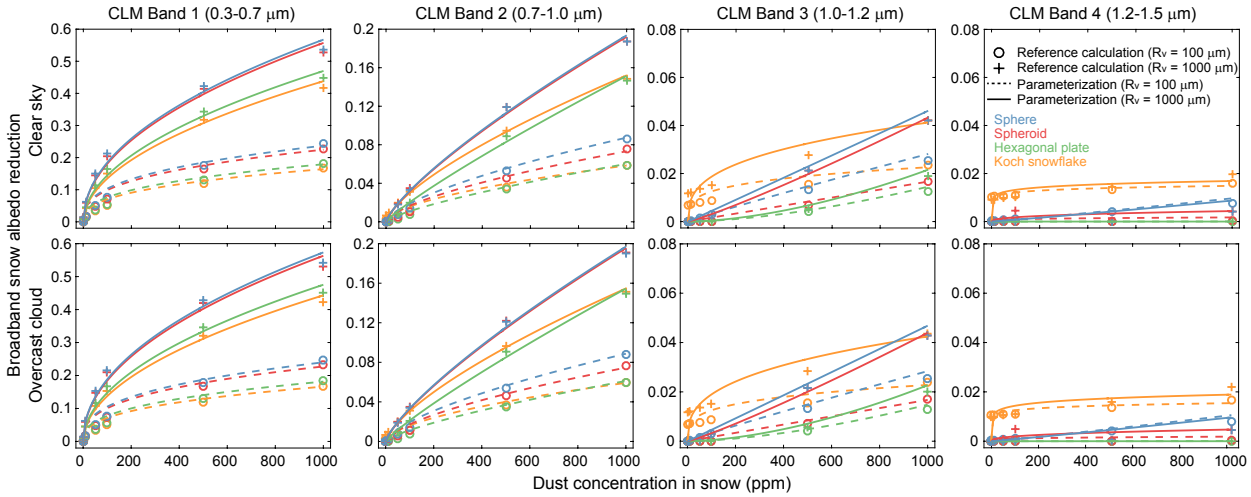

Figure S8. Broadband snow albedo reduction ($\Delta\alpha$) under clear-sky (top row) and overcast-cloud (bottom row) conditions as a function of dust concentration in snow from reference calculations (points) and parameterizations (Equations 2–4; lines) for dust-snow internal mixing at the Community Land Model (CLM) bands. Results shown here are for snow volume-equivalent sphere radii (R_v) of 100 μm (circles or dashed lines) and 1000 μm (crosses or solid lines) and four grain shapes, including sphere (blue), spheroid (red), hexagonal plate (green), and Koch snowflake (orange). Results at wavelength bands of >1.5 μm are not shown due to negligible dust-induced albedo reduction. Note that differences in broadband snow albedo reductions between clear-sky and overcast-cloud conditions are small due to similar characteristics of incoming solar spectra under the two conditions.

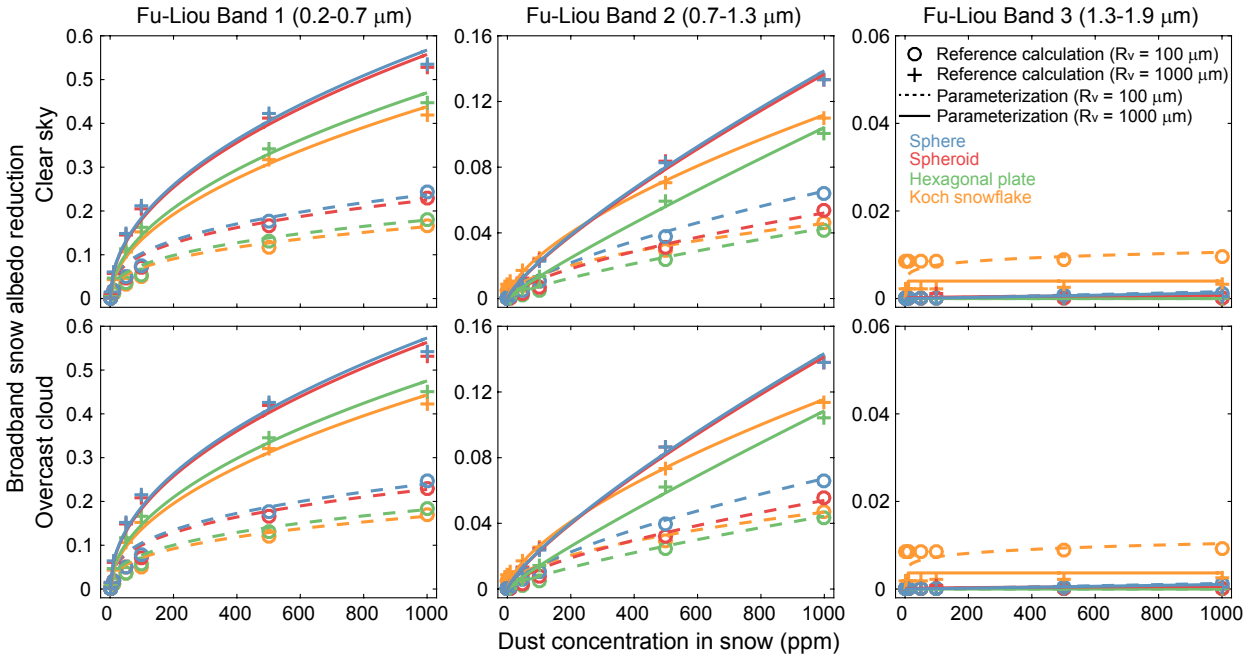

Figure S9. Same as Figure S8, but for the Fu-Liou bands. Results at wavelength bands of >1.9 μm are not shown due to negligible dust-induced albedo reduction.

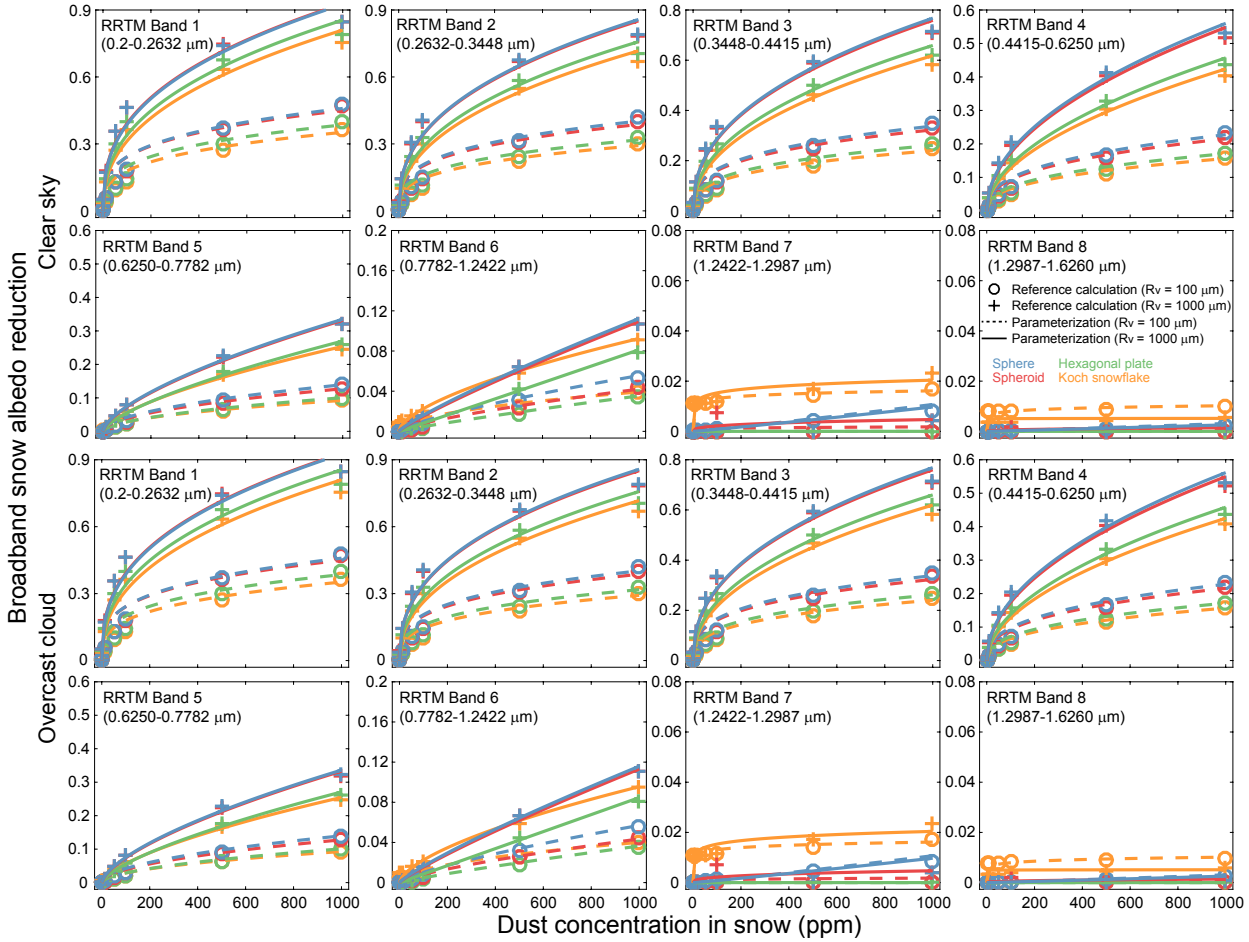

Figure S10. Same as Figure S8, but for the Rapid Radiative Transfer Model (RRTM) bands. Results at wavelength bands of >1.626 μm are not shown due to negligible dust-induced albedo reduction.

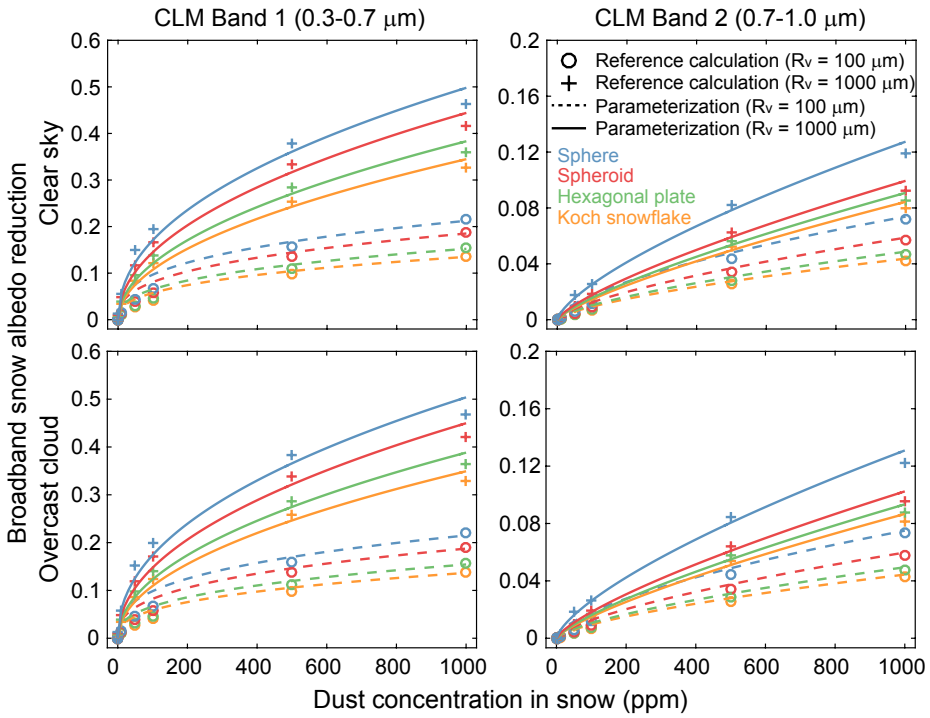

Figure S11. Same as Figure S8, but for the dust-snow external mixing. Results at wavelength bands of >1.0 μm are not shown due to negligible dust-induced albedo reduction.

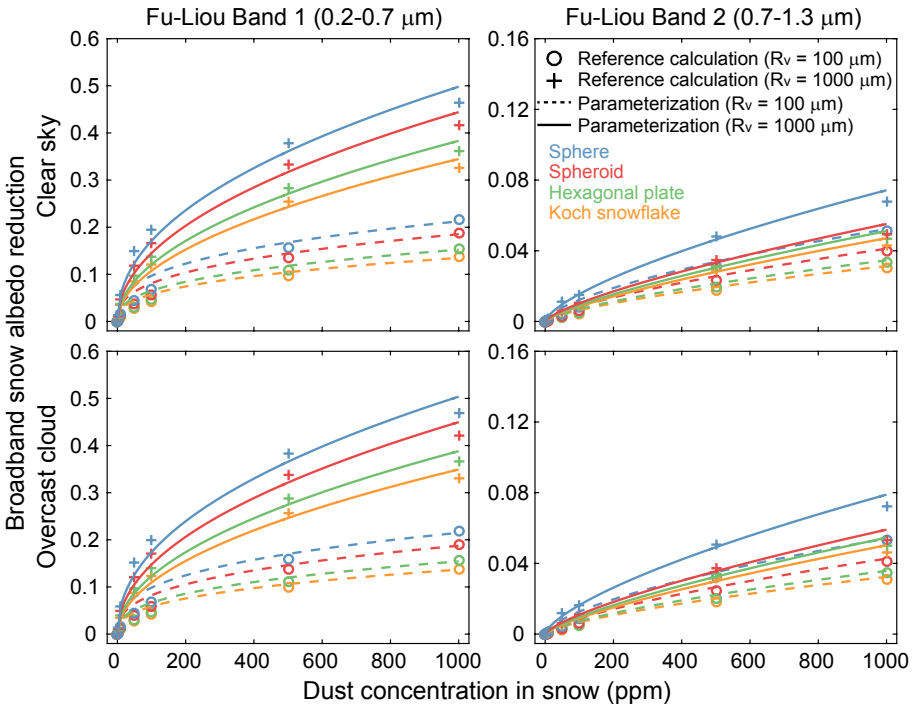

Figure S12. Same as Figure S11, but for the Fu-Liou bands. Results at wavelength bands of >1.3 μm are not shown due to negligible dust-induced albedo reduction.

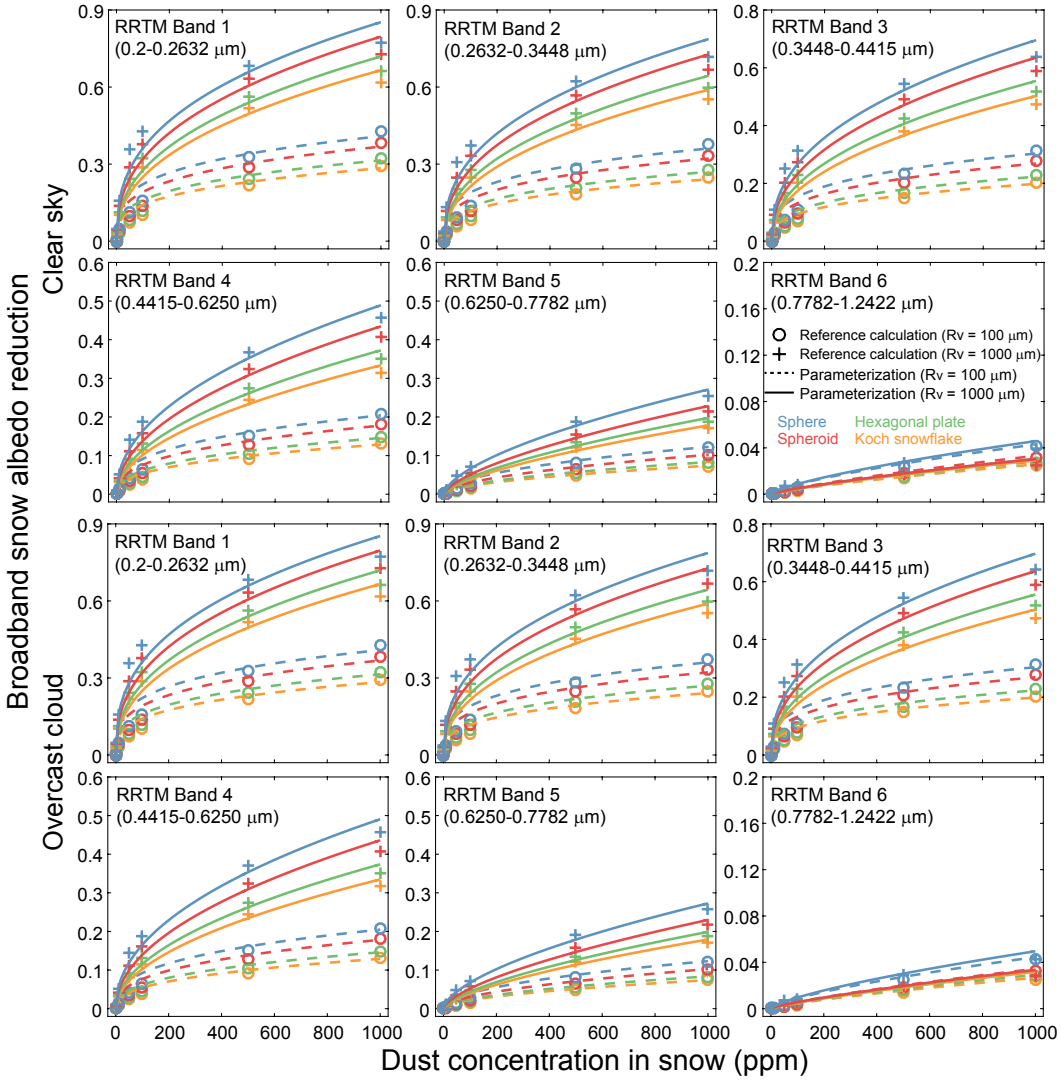

Figure S13. Same as Figure S11, but for the Rapid Radiative Transfer Model (RRTM) bands. Results at wavelength bands of >1.2422 μm are not shown due to negligible dust-induced albedo reduction.

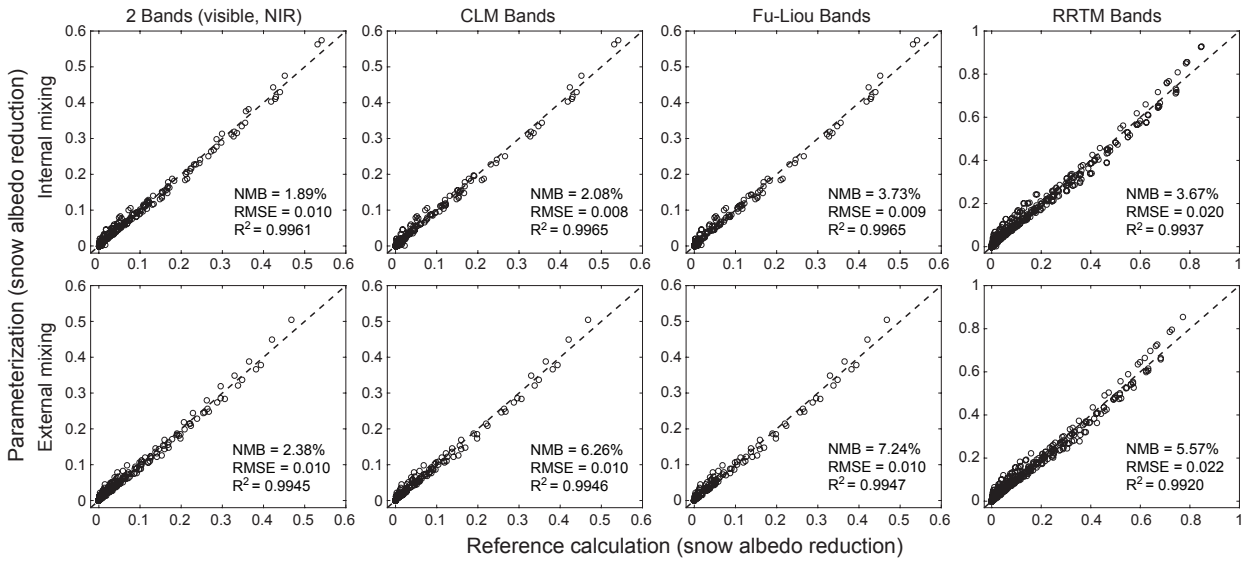

Figure S14. Comparisons of broadband snow albedo reduction ($\Delta\alpha$) under the overcast-cloud condition caused by dust-snow internal (top row) and external (bottom row) mixing from reference calculations and parameterizations (Equations 2–4) for different snow grain shapes (i.e., sphere, spheroid, hexagonal plate, and Koch snowflake) and volume-equivalent sphere radii (i.e., 100, 500, and 1000 mm). Results at different wavelength bands are shown, including the visible (0.3–0.7 μm)-NIR (0.7–5.0 μm) bands (1st column), the Community Land Model (CLM) bands (2nd column), the Fu-Liou bands (3rd column), and the Rapid Radiative Transfer Model (RRTM) bands (4th column). Also shown are the normalized mean bias (NMB), the root-mean-square-error (RMSE), the coefficient of determination (R^2), and the 1:1 ratio lines (dashed lines).

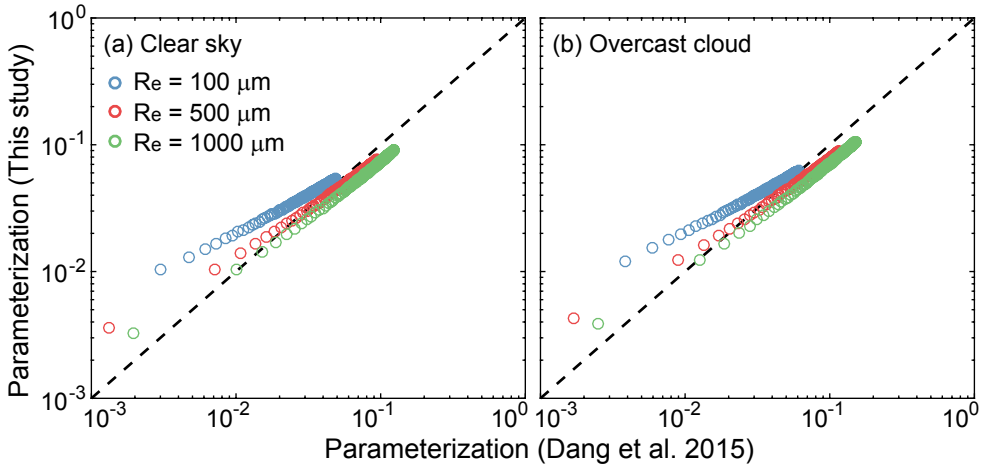

Figure S15. Comparison of broadband (0.3–5.0 μm) snow albedo reduction caused by dust-snow external mixing from the Dang et al. (2015) parameterization and this study's parameterization under (a) clear-sky and (b) overcast-cloud conditions for snow spheres with effective radii (R_e) of 100 μm (blue), 500 μm (red), and 1000 μm (green). Circles are results assuming dust concentrations of 0.1–100 ppm (with an interval of 1 ppm) in snow. Note that the Dang et al. (2015) parameterization is not applicable to very large dust concentrations (>100 ppm). Also shown are the 1:1 ratio lines.

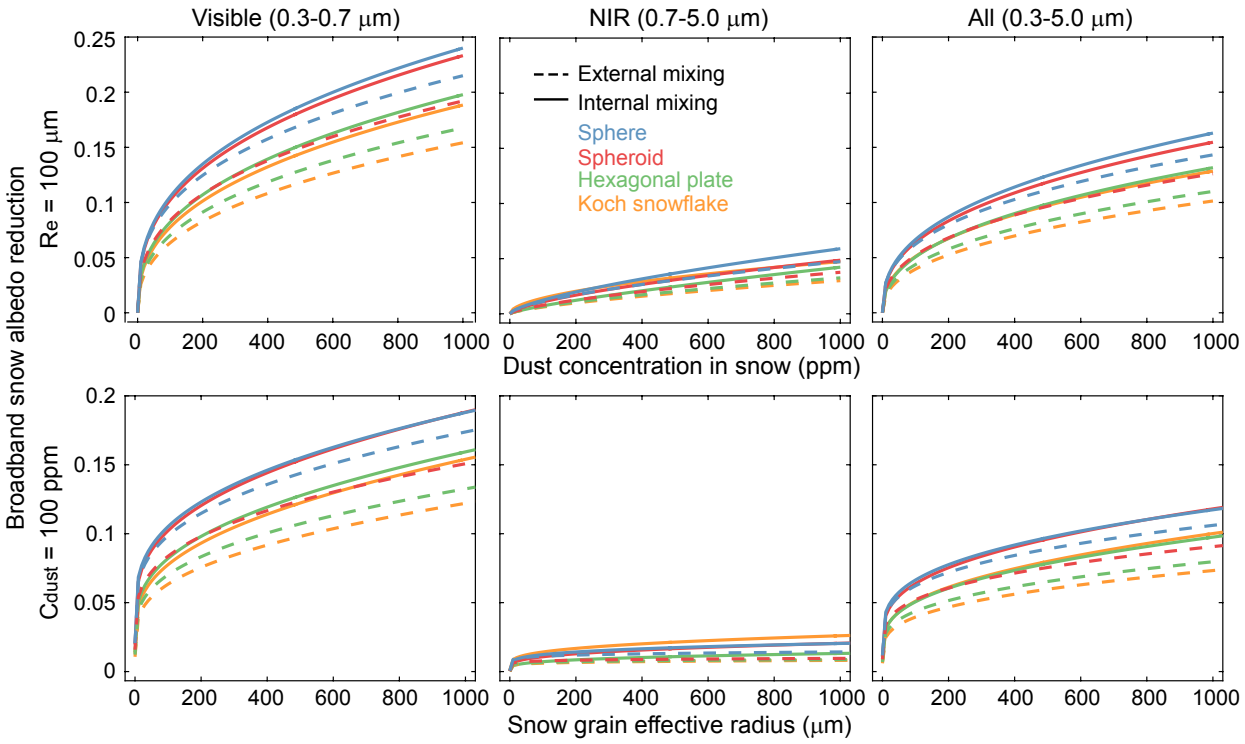

Figure S16. Top row: Broadband snow albedo reduction ($\Delta\alpha$) under the overcast-cloud condition as a function of dust concentration in snow based on the parameterization (Equations 2–4) for dust-snow internal (solid lines) and external (dashed lines) mixing with a snow grain effective radius (R_e, defined in Equation 4) of 100 μm. Results shown here are for snow sphere (blue), spheroid (red), hexagonal plate (green), and Koch snowflake (orange) at the visible (0.3–0.7 μm; 1st column), near-infrared (NIR, 0.7–5.0 μm; 2nd column), and all-wavelength (All, 0.3–5.0 μm; 3rd column) bands. Bottom row: Same as Figure S13 (top row), but for snow albedo reduction as a function of snow grain effective radius (R_e) with a dust concentration in snow (C_{dust}) of 100 ppm.

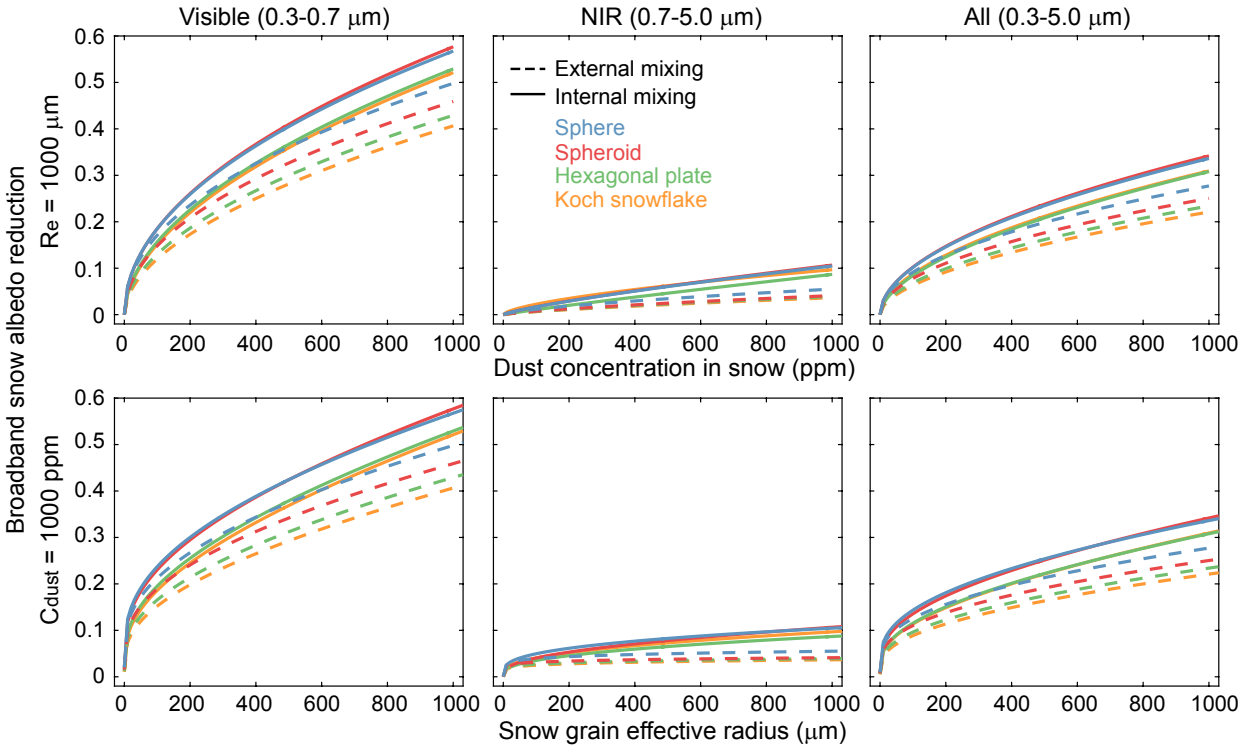

Figure S17. Same as Figure S16, but for clear-sky snow albedo reduction with a snow grain effective radius (R_e) of 1000 μm and a dust concentration in snow (C_{dust}) of 1000 ppm.

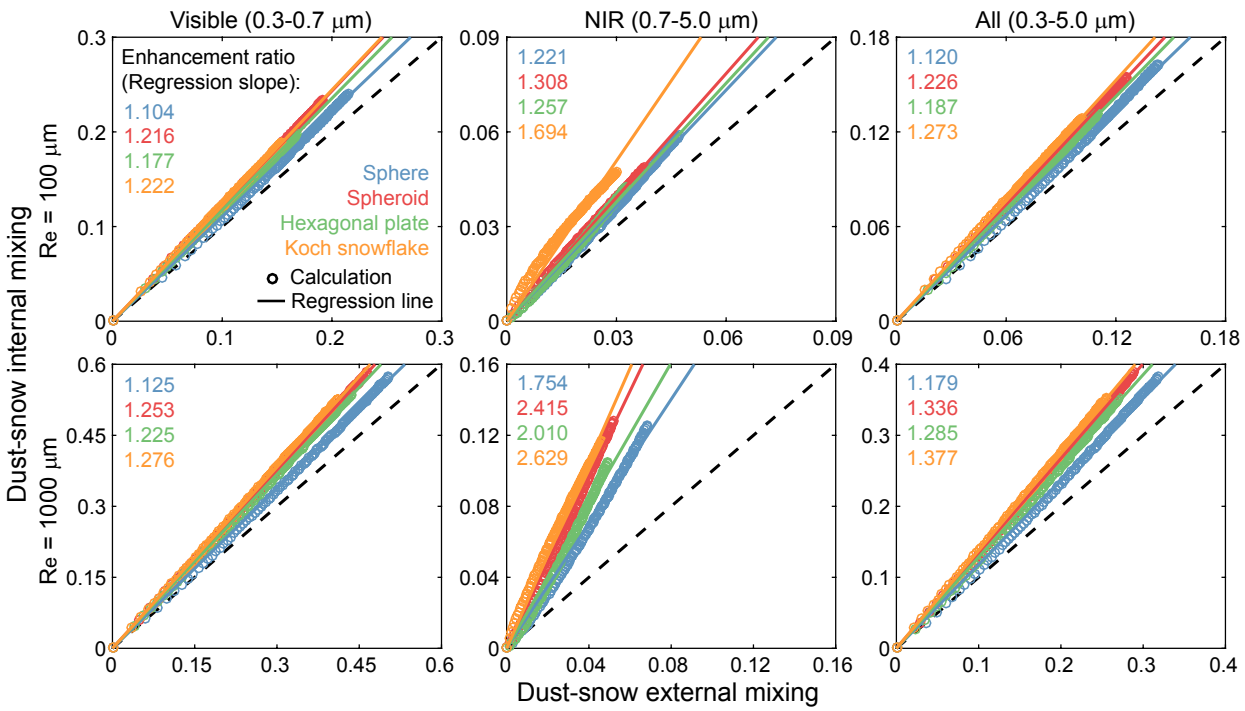

Figure S18. Comparisons of snow albedo reduction ($\Delta\alpha$) under the overcast-cloud condition caused by dust-snow internal mixing (y-axis) and external mixing (x-axis) for snow sphere (blue), spheroid (red), hexagonal plate (green), and Koch snowflake (orange) with grain effective radii (R_e, defined in Equation 4) of 100 μm (top row) and 1000 μm (bottom row) at the visible (0.3–0.7 μm; 1st column), near-infrared (NIR, 0.7–5.0 μm; 2nd column), and all-wavelength (All, 0.3–5.0 μm; 3rd column) bands. Circles are calculated results assuming dust concentrations of 0–1000 ppm (with an interval of 10 ppm) in snow. Also shown are linear regression lines (solid lines) and regression slopes (enhancement ratio, $E_{\Delta\alpha}$ defined in Equation 5; colored numbers) for each snow grain shape (see also Table 3).

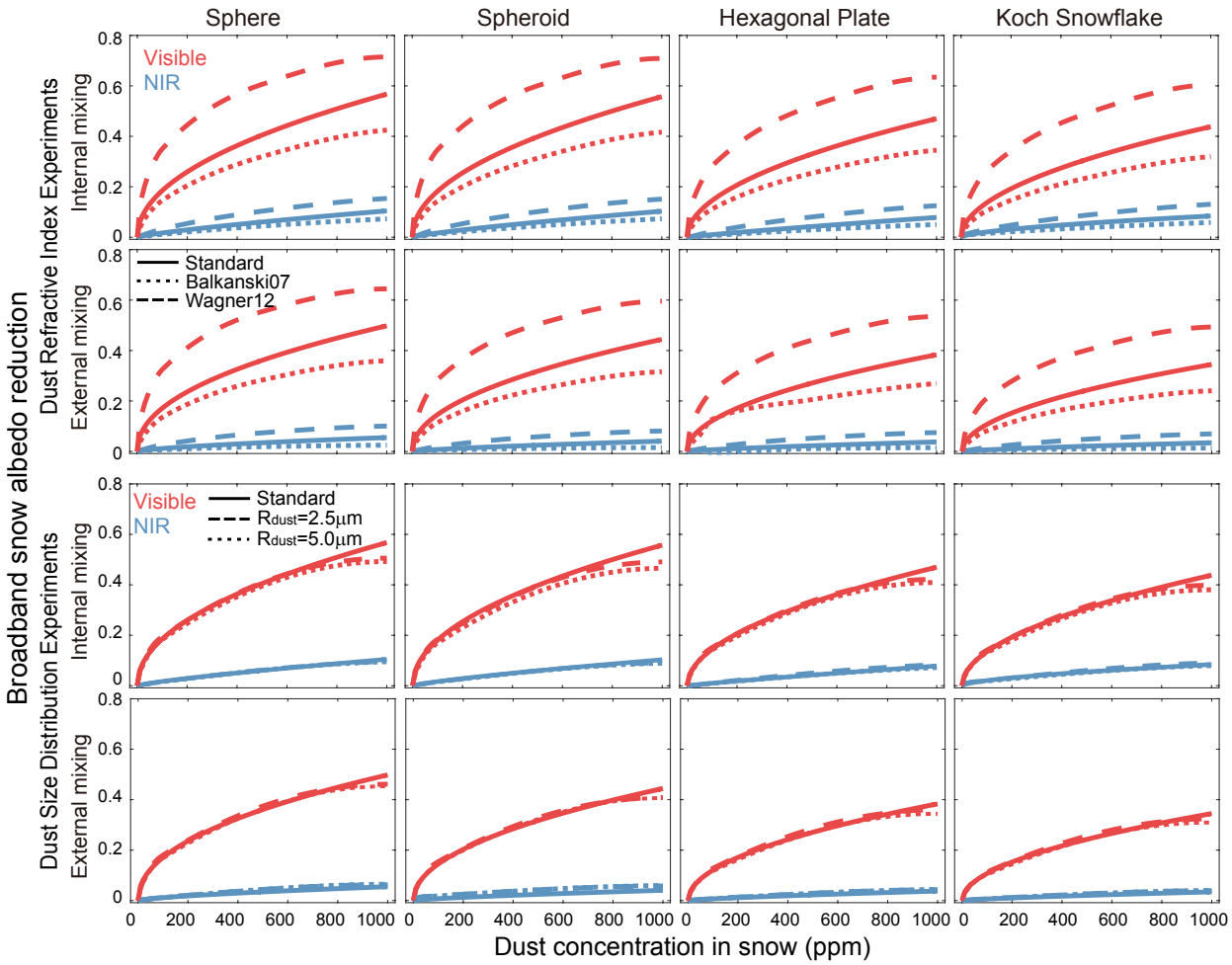

Figure S19. Clear-sky visible (0.3–0.7 μm; red) and near-infrared (NIR, 0.7–5.0 μm; blue) broadband snow albedo reduction as a function of dust concentration in snow for dust-snow internal (first and third rows) and external (second and fourth rows) mixing for sphere (first column), spheroid (second column), hexagonal plate (third column), and Koch snowflake (fourth column) with a snow volume-equivalent sphere radius of 1000 μm, based on sensitivity simulations by varying dust refractive indices (top two rows) and size distributions (bottom two rows). In top two rows, the dashed and dotted lines represent results using spectral dust imaginary refractive indices from the Wagner et al. (2012) and Balkanski et al. (2007) databases, respectively, compared with spectral dust imaginary refractive indices from the Dang et al. (2015) database used in standard simulations (solid lines). In bottom two rows, the dashed and dotted lines represent results using dust effective radii (R_{dust}) of 2.5 and 5.0 μm, respectively, compared with a R_{dust} of 1.1 μm used in standard simulations (solid lines).

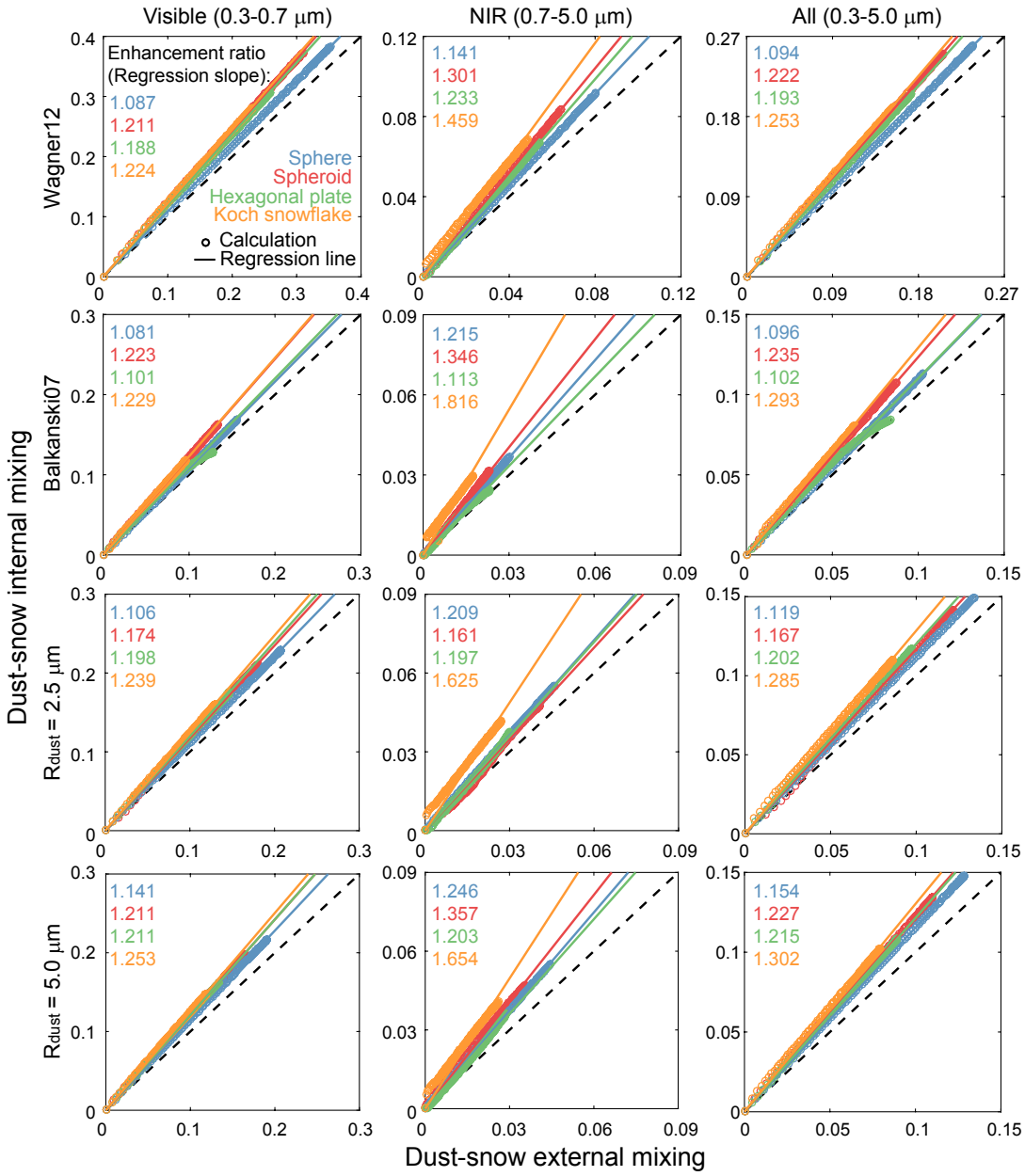

Figure S20. Same as Figure S18 (standard simulations), but for different sensitivity simulations with a snow volume-equivalent sphere radius of 100 μm under the overcast-cloud condition. The top two rows are results using spectral dust imaginary refractive indices from the Wagner et al. (2012) and Balkanski et al. (2007) databases, respectively. The bottom two rows are results using dust effective radii (R_{dust}) of 2.5 and 5.0 μm, respectively.

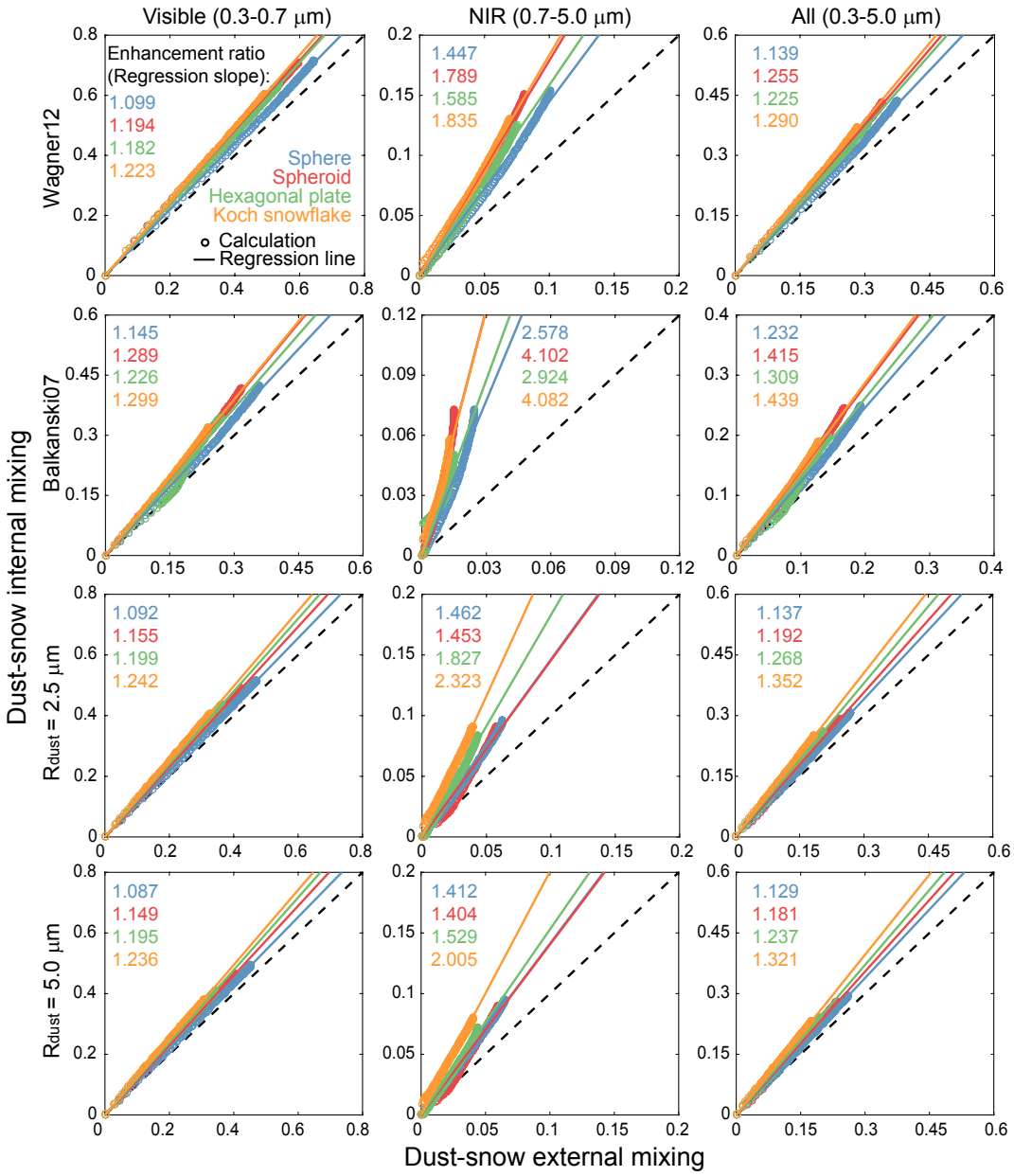

Figure S21. Same as Figure S20, but for a snow volume-equivalent sphere radius of 1000 μm under the clear-sky condition.

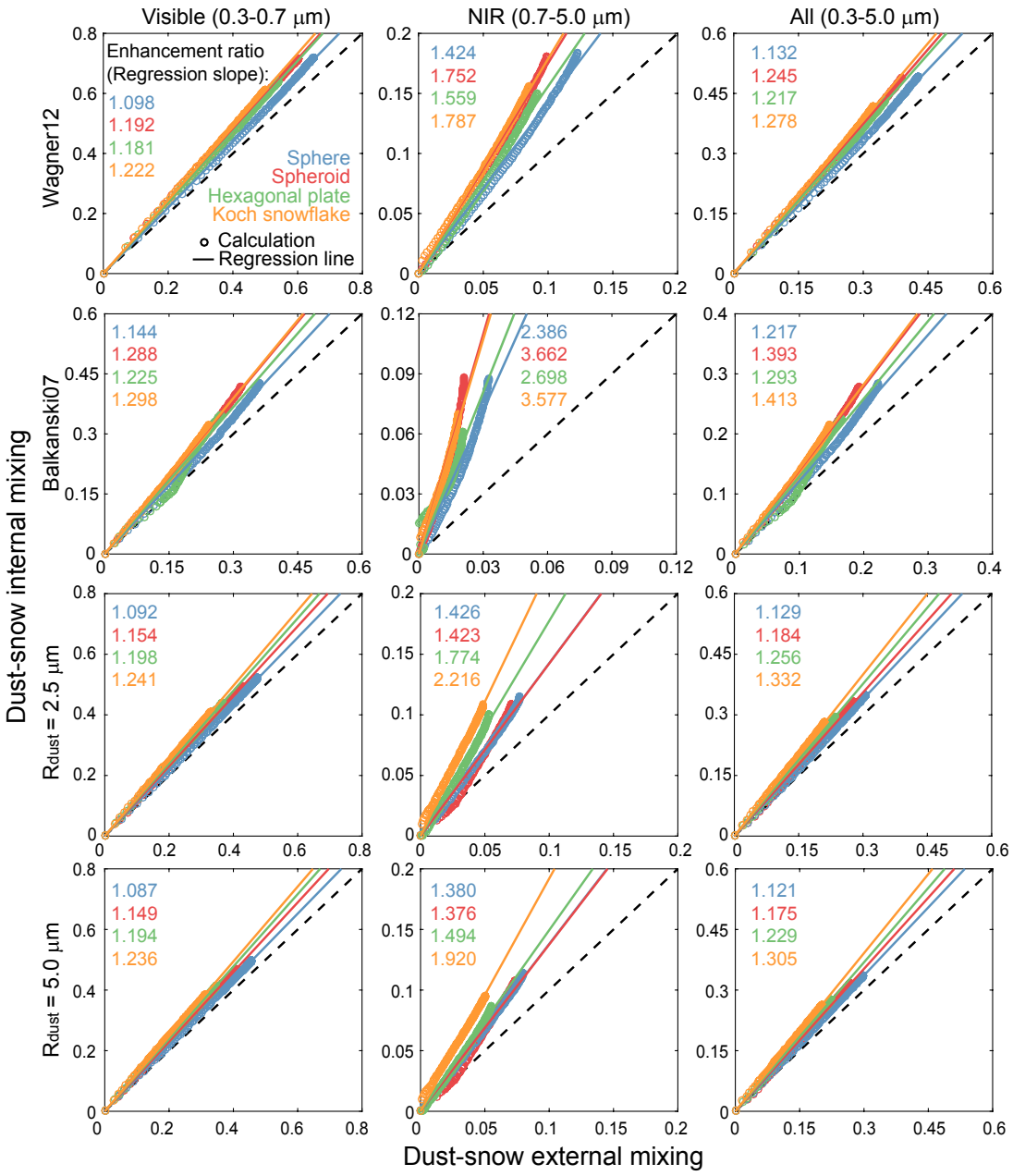

Figure S22. Same as Figure S20, but for a snow volume-equivalent sphere radius of 1000 μm under the overcast-cloud condition.